ACS APPLIED MATERIALS & INTERFACES

Research Article

www.acsami.org

Surface Ferromagnetic p-Type ZnO Nanowires through Charge Transfer Doping

Sung-Hoon Lee,*[,†] Jongseob Kim,[†] Ki-Ha Hong,[‡] Jaikwang Shin,[†] Sungjin Kim,[†] and Kinam Kim[†]

[†]Samsung Advanced Institute of Technology, Yongin 446-712, Korea

[‡]Department of Materials Science and Engineering, Hanbat National University, Daejeon 305-719, Korea

ABSTRACT: We report first-principles theoretical investigation of p-type charge transfer doping of zinc oxide (ZnO) nanowires by molecular adsorption. We find that spontaneous dissociative adsorption of fluorine molecules introduces half-emptying of otherwise fully filled oxygen-derived surface states. The resulting surface Fermi level is so close to the valence band maximum of the ZnO nanowire that the nanowire undergoes significant p-type charge transfer doping. Those half-filled surface states are fully spin-polarized and lead to surface ferromagnetism that is stable at room temperature. We also analyze the kinetic control regime of the surface transfer doping and find that it may result in nonequilibrium steady states. The present results suggest that postgrowth engineering of surface states has high potential in manipulating ZnO nanostructures useful for both electronics and spintronics.

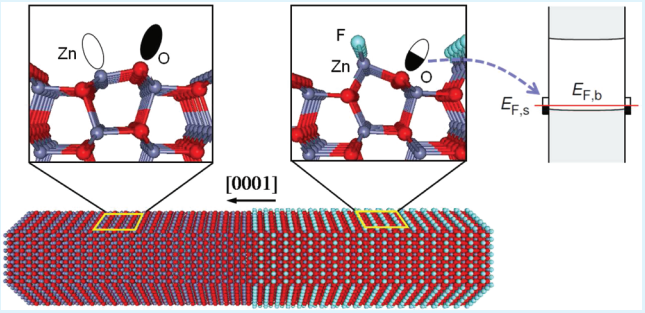

KEYWORDS: *surface transfer doping, surface ferromagnetism, surface states, ZnO, nanowires*

INTRODUCTION

The electronic properties of semiconducting materials have been controlled usually by introducing small amount of impurity atoms into the bulk, which have additional charge carriers such as electrons or holes.[1] Semiconductor nanostructures[2−7] that show high surface-to-volume ratios have another degree of freedom to control their electronic properties. Electronic states localized at surfaces can play as donor or acceptor levels, depending on their energy level and occupation.[8−10] The control of surface states thus has strong implication for the application of semiconductor nanostructures to electronics. This surface state engineering can be especially useful for materials where the control of electronic properties in bulk is difficult, such as ZnO.

ZnO has been celebrated for the past decade as photonic materials owing to the wide band gap, high exciton binding energy, and availability of large bulk single crystals.[11−13] Despite the high potential of ZnO, its application has been hindered by the difficulty to obtain p-type doping, mainly due to high acceptor levels and low solubility of p-type dopants.[12,13] For example, nitrogen defects substituting oxygen have an acceptor level of 0.4 eV,[14] whereas most effective dopants for Si have acceptor levels of less than 0.1 eV.[1] To overcome the p-type doping difficulty, various efforts have been made.[15−17] Although there have been successful reports on p-type impurity doping for ZnO, controversies still pervade and reproducible and stable p-type doping has remained challenging.[18,19]

ZnO has attracted much interest also for spintronic applications. An early theoretical proposal[20] suggested that room-temperature ferromagnetism is possible for p-type doped ZnO with transition metal impurities, where holes mediate magnetic coupling between localized magnetic moments.[21,22] Many experimental studies have been performed and reported room-temperature ferromagnetism.[23−26] However, there is no consensus yet whether it is really due to hole mediation or due to extrinsic factors such as impurity clustering, defects in grain boundaries, or other structural defects.[26−28] Interestingly, recent studies[29−32] found that even without magnetic impurities, nanostructures of ZnO exhibit room-temperature ferromagnetism. The detailed origin is unknown, but it is highly probable that surface states have played a role for the ferromagnetic order[33] owing to enhanced localization at surfaces. This suggests that engineering surface states could be a useful tool for spintronic applications of ZnO.

In this paper, we investigate the possibility of surface state engineering for ZnO nanowires. Performing first-principles calculations and solving the Poisson−Boltzmann equation, we show that postgrowth F_2 adsorption modifies the surface electronic structure to allow both p-type charge transfer doping and surface ferromagnetism simultaneously. We examine first the utility of charge transfer doping for ZnO nanowires, and discuss our scheme for the p-type charge transfer doping of ZnO nanowires using molecular adsorption. The following first-principles calculation results show that fluorine adsorption produces p-type doping of ZnO nanowires. Before we show that fluorine-adsorbed surfaces have two-dimensional ferro-

Received: November 22, 2011
Accepted: February 2, 2012
Published: February 2, 2012

   dx.doi.org/10.1021/am201633x | *ACS Appl. Mater. Interfaces* 2012, 4, 1365−1370

magnetic ordering that is stable at room temperature, we examine the kinetic aspect of the p-type surface transfer doping when it is applied to n-type ZnO nanowires. Finally, we discuss the potential applications of this postgrowth surface treatment method.

RESULTS AND DISCUSSION

Scheme. We first examine the utility of a charge transfer doping scheme for ZnO nanowires. Charge transfer doping by surface states[8−10] is illustrated in Figure 1a for p-type doping of

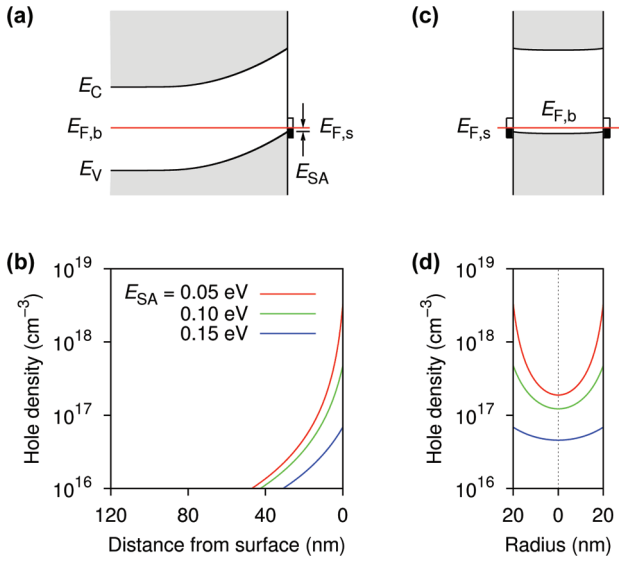

Figure 1. Influence of surface states on semiconductor doping. (a) Schematic band diagram of an undoped semiconductor with empty surface states. Electrons in the valence band of the semiconductor body moves to the empty surface states by thermal excitation, leaving holes in the semiconductor body. The difference between the surface Fermi energy $E_{F,s}$ and the valence band maximum E_V at the surface can be defined as an effective acceptor energy for the surface states, E_{SA}. (b) Calculated hole density as a function of the surface acceptor energy E_{SA}. (c) Band diagram for a semiconductor nanowire of a diameter of 40 nm. (d) Calculated radial hole density for the nanowire. The body is in p-type with high hole densities at the center.

undoped semiconductors. If a semiconductor has low-energy empty surface states close to the valence band maximum (E_V), then electrons in the valence band move to the surface states by thermal excitation, until charge-transfer-induced band bending leads to a balance between the Fermi level (E_F) inside and at surfaces (Figure 1a). This electron transfer, determined by electrostatics and Fermi statistics, leaves free holes in the semiconductor body near surfaces. To achieve a high density of holes, the empty surface states need to be close to E_V in energy, as shown in Figure 1b, and also of high density so that E_F at the surface would not increase significantly by the electron transfer. In the energy band diagram calculations, the carrier densities are obtained by solving the Poisson equation with electron and hole densities satisfying the Boltzmann relations.[1] As ZnO material parameters, we use the bandgap energy of 3.4 eV, the dielectric constant of 8.7, the effective mass and band degeneracy of 0.24 and 1 for the conduction band, and 0.59 and 2 for the valence band.[12] The density of surface states is assumed to be high enough to neglect the change in the surface Fermi energy $E_{F,s}$ by the electron transfer. For bulk semiconductors, the use of charge transfer doping is limited in thin regions of surfaces. But it can greatly increase for nanostructures, where the Fermi energy inside the nanowire is strongly affected by surface states (Figure 1c). Calculations show that nanowires of 40 nm thick is fully p-type doped with a hole density of above 1×10^{17} cm^{-3} at the center if the surface acceptor level is below 0.1 eV (Figure 1d).

In vertically aligned nanowire arrays, a typical example of ZnO nanostructures,[2,3] each ZnO nanowire grows along the *c*-axis in the wurtzite structure with a hexagonal cross-section and six equivalent $(10\bar{1}0)$ side surfaces[3,34] (Figure 2a). The

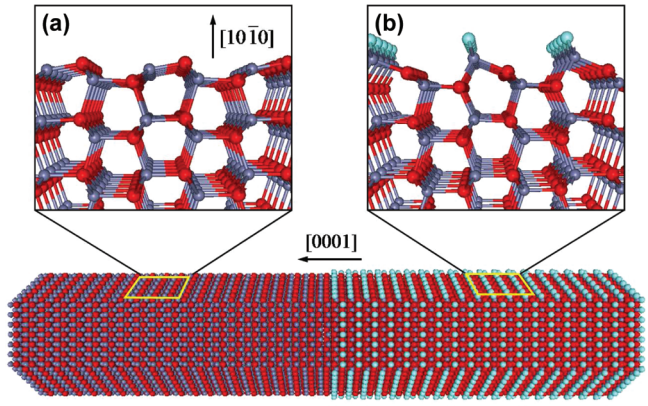

Figure 2. Atomic structure of ZnO nanowires, which grows in the wurtzite structure along the [0001] direction. (a) Atomic structure of the ZnO$(10\bar{1}0)$ surface. (b) Atomic structure of the F-adsorbed ZnO$(10\bar{1}0)$ surface. Red, blue, and cyan spheres represent O, Zn, and F atoms, respectively.

nonpolar side surface is characterized by tilted ZnO dimers.[35] The tilt comes from electronic relaxation to relieve broken bonds of surface atoms: Electrons in Zn dangling bonds move to lower-energy O dangling bonds. This leaves empty Zn dangling bonds above the conduction band minimum E_C and occupied O dangling bonds around E_V (Figure 3a), which is typical to nonpolar surfaces of III−V or II−VI compound semiconductors.[36,37] Thus, the bare surfaces of ZnO nanowires do not possess electron-trapping surface states relevant to p-type doping. To induce p-type charge transfer doping on this surface, one may consider molecular overlayers with low-energy empty molecular orbitals.[10,38] But, because E_V of ZnO is as deep as ∼8 eV from the vacuum level, due to highly electronegative O atoms, surface acceptor molecules need to have lowest unoccupied molecular orbital (LUMO) levels at such a low energy, which is unachievable for most molecules.

Our approach to introduce empty surface states near E_V on the ZnO surface involves chemical adsorption of atomic or molecular species whose highest occupied molecular orbital (HOMO) is singly occupied (Figure 3). The singly occupied molecular orbital (SOMO) of the adsorbing species makes hybrid levels with a Zn dangling bond, and the bonding hybrid level is singly occupied. If the singly occupied hybrid level is lower in energy than the O dangling bonds, then electrons in the latter move to fill out the former. In this case, the O dangling bonds would be singly occupied and play as surface acceptor states. The adsorbing species would not bind to surface O atoms because it requires filling of antibonding hybrid levels and thus is energetically unfavorable. To make this doping scheme work, there are conditions to be satisfied. First, the SOMO energy level of adsorbing species is sufficiently low, that is, the adsorbing atoms or molecules are highly

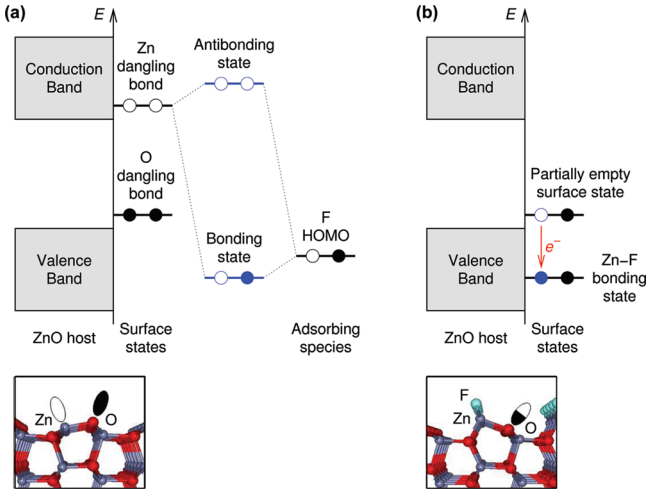

Figure 3. Scheme to introduce surface acceptor states at the nonpolar ZnO surface by chemical adsorption. (a) Band diagram of the clean surface and its coupling with an adsorbing species having a low-energy singly occupied HOMO, here a F atom. (b) Band diagram of the resulting F-adsorbed surface. The surface state near the valence band, filled at the clean surface, becomes partially empty by the F adsorption. Lower panels show the atomic structures of the clean and F-adsorbed surfaces with schematic drawing of surface dangling bonds.

electronegative. Second, the binding of adsorbates at the surface is strong enough not to be broken easily. Last, the bond between the adsorbate and the substrate is easy to form through barrierless and exothermic reactions. As such surface dopant species, we considered fluorine.

Calculation Methods. The reaction of fluorine, available as gas-phase diatomic molecules (F_2), with the ZnO surface is quantitatively analyzed using first-principles calculations based on the density functional theory (DFT) employing the generalized gradient approximation[39] and the projector-augmented-wave method as implemented in VASP.[40,41] Valence electronic wave functions are expanded in a planewave basis set with a cutoff energy of 400 eV. The equilibrium lattice parameters for wurtzite ZnO are calculated to be a = 3.151 Å, c = 5.068 Å, and u = 0.380. The nonpolar $(10\bar{1}0)$ surface is represented by a periodic slab containing 20 ZnO layers. The bottom layer is passivated with artificial atoms having a valence of 1.5 and 0.5 for Zn and O atoms, respectively, so that the bottom side does not affect the molecular interaction of the top surface. The k-point integration over the (1×1) surface Brillouin zone uses a uniform 4×6 sampling. The atomic positions of twelve topmost layers are relaxed until residual forces are less than 0.02 eV/Å. The bandgap underestimation is partly corrected by adopting the GGA+U scheme[42] with an onsite Coulomb repulsion parameter U of 8 eV for the Zn d orbital. Spin-polarized calculations are used for F adsorbed ZnO surfaces.

Energetics. When the surface is exposed to fluorine gas, F_2 molecules are attracted to Zn sites and dissociate spontaneously without transition barriers. Each of dissociated F atoms forms a bridge bond with two Zn atoms. The adsorption energy gain is as high as 2.9 eV per molecule. The high energy gain and reactivity are largely maintained until the density of adsorbed F atoms is one per each surface Zn atom. When additional F_2 molecules are incorporated, they interact only weakly with the surface: Their binding energy is below 0.1 eV, weak enough for vacuum pumping after the exposure of fluorine gas to purge away those weakly adsorbed molecules. The resulting fully F-adsorbed surface shows a reversed tilt in the Zn−O dimer (Figure 3b), indicating charge transfer from surface O dangling bonds to Zn−F bonds.

Band Structures. Figure 4 shows the calculated electronic structures of the clean and F-adsorbed ZnO surfaces. They are in agreement with the schematic energy diagrams in Figure 3, except for the energy level broadening of surface states due to their wave function overlap. The surface states near E_V, derived mainly from O atoms in the surface ZnO double layer, are filled in the clean surface and partially empty after the F adsorption. At this point, we emphasize that the emptied surface states by themselves do not mean the hole states. Those surface states are, while extended over the surface, strongly localized in the surface normal direction, largely within a couple of atomic layers. The transport through them suffers from scattering with surface defects and steps and has much smaller mobility than that through the valence band of the semiconductor body.[9,10] The emptiness of surface states here implies that they can accept electrons from the valence band of the semiconductor body and thus generate holes there.

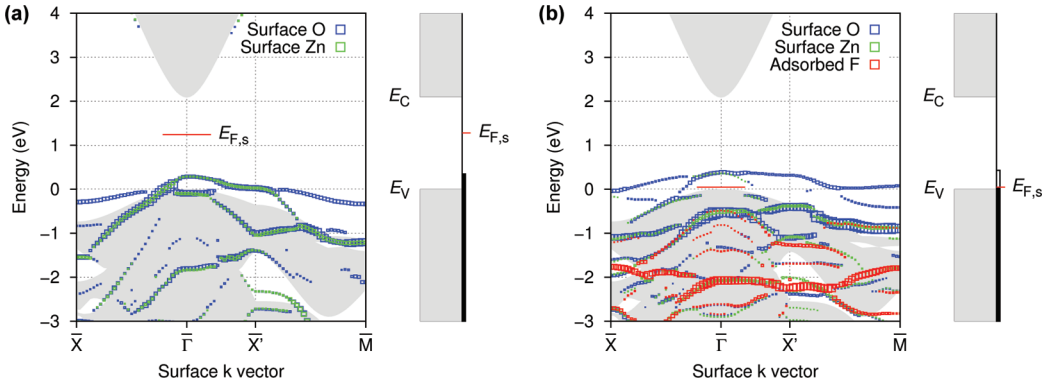

Figure 4. Electronic band structures of the ZnO $(10\bar{1}0)$ surfaces. (a) Electronic band structure of the clean surface along the surface k vectors of the high symmetry line of the surface Brillouin zone. Square symbols indicate electronic states having a substantial contribution from the atoms in the surface ZnO double layer. Larger symbols reflect higher contribution. Gray regions indicate electronic states derived from bulk atoms. The bulk valence band maximum is set to be zero. The electronic states within the bulk bandgap are derived mainly from surface oxygen atoms and fully occupied. In the right, a simplified diagram of the surface-k-vector-resolved band structure is given. (b) Electronic band structure of the fully F-adsorbed surface. F-derived states are located at ∼2 eV below E_V. The surface Fermi level $E_{F,s}$ iss 0.05 eV above E_V.

dx.doi.org/10.1021/am201633x | ACS Appl. Mater. Interfaces 2012, 4, 1365−1370

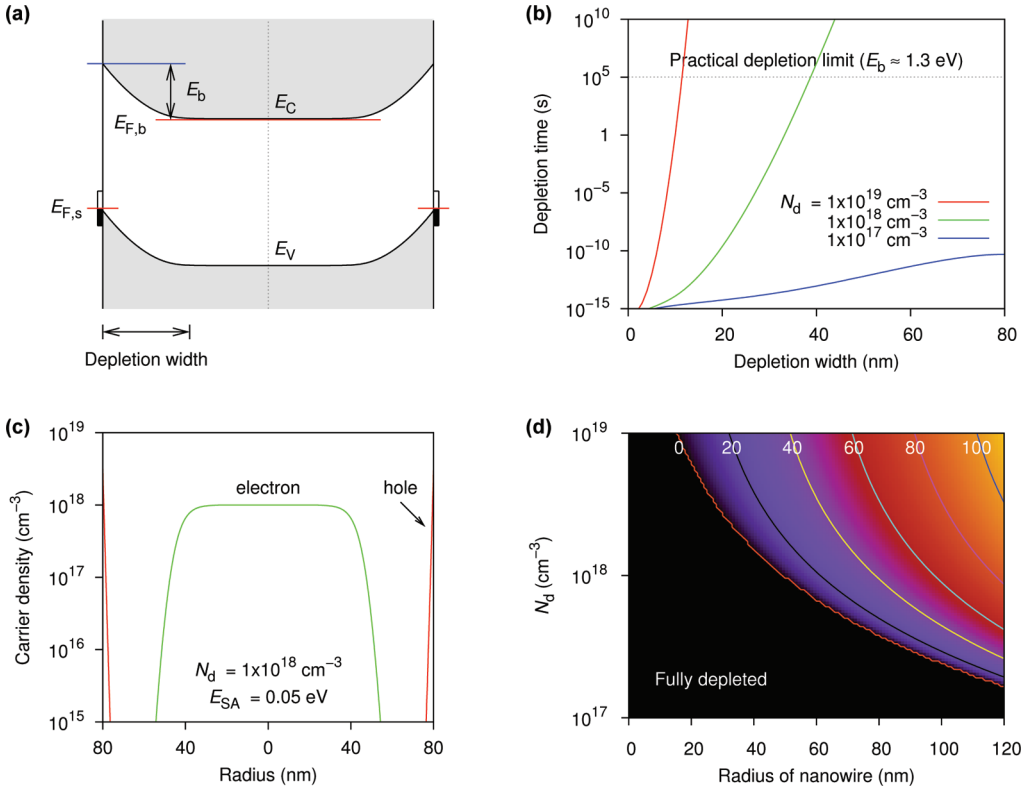

Figure 5. p-type surface transfer doping applied to n-type impurity-doped nanowires: Nonequilibrium steady states. (a) Band diagram before thermal equilibrium is reached, i.e., $E_{F,b} \neq E_{F,s}$. Electron transfer from the bulk conduction band to the surface states gives rise to a diffusion barrier (E_b) that hinders thermal equilibrium. (b) Depletion time as a function of the depletion width, calculated at room temperature. The nanowire radius is 80 nm. N_d is the n-type doping concentration of the nanowire. For high N_d, as the depletion width and thus E_b increases, the depletion time increases very rapidly, resulting in nonequilibrium steady states in practice. (c) Carrier density distribution at the nonequilibrium steady state with $E_b \simeq 1.3$ eV. Here the surface acceptor level $E_{SA} \equiv E_{F,s} - E_V$ is 0.05 eV. The nanowire has two conduction paths, n-type core and p-type surface shell, forming a radial p-n junction. (d) Contour plot of the n-type core size (in nm) at the nonequilibrium steady state as a function of nanowire radius and N_d. Only when the nanowire radius is small or N_d is low, electrons in the nanowire conduction band are fully depleted.

The calculated surface Fermi level ($E_{F,s}$) of the F-adsorbed surface is low enough to give significant hole population. At the saturation coverage, the surface acceptor level ($E_{F,s}-E_V$) is 0.05 eV. Moreover, it is almost pinned at the value owing to the high density of surface states of about 1×10^{15} cm^{-2}eV^{-1}, which is typical for a surface unit-cell of ~10 Å^2 and a bandwidth of ~1 eV. $E_{F,s}$ changes upward by the electron transfer only by several meV, even assuming the maximum transfer (to yield a band bending of E_g). Thus the present first-principles results combined with the band diagram calculations in Figure 1d show that the surface transfer doping scheme can indeed produce a significant hole population for ZnO nanowires of diameters of up to ~100 nm.

Kinetics. This surface transfer p-type doping scheme needs caution when it is applied to n-type doped ZnO nanowires. There are self-limiting effects that prevent the system from reaching thermal equilibrium shortly. The n-type doping of ZnO can occur unintentionally in most growth conditions by hydrogen impurities.[43,44] Upon the formation of surface acceptor states by F adsorption, electrons in the nanowire conduction band diffuse to surfaces and are trapped in the surface states. This charge transfer continues until the resulting band bending equilibrates the Fermi levels inside the nanowire and at the surface. The problem is that because band bending builds up an energy barrier for electron diffusion (Figure 5a), this diffusion process is self-limiting and may require a prohibitively long time to reach thermal equilibrium.

Figure 5b shows the time to deplete electrons of n-type doped nanowires of 80 nm radius as a function of the depletion width (W_D) at room temperature. Here, the depletion time T is calculated within the depletion approximation[1] by

$$T(W_D) = \int_0^{W_D} \frac{qN_d}{2\pi Rj(w)} 2\pi(R - w)dw$$

where q is the electric charge, N_d is the n-type doping concentration, R is the nanowire radius, and $j(w)$ is the thermionic emission current to the surface when the depletion width is w. When a nanowire of 80 nm radius is lightly n-type doped, e.g., $N_d = 1 \times 10^{17}$ cm^{-3}, the diffusion barrier grows slowly and the full depletion of electrons in the nanowire conduction band is achieved shortly. But when the doping concentration is moderate or high, the depletion time grows rapidly. For $N_d = 1 \times 10^{18}$ cm^{-3}, it takes more than 1×10^{10} s for full depletion. So the system would remain in practice at a nonequilibrium steady state: The depletion width saturates at ~40 nm with an n-type core of ~40 nm radius (Figure 5c), which would be fully depleted at thermal equilibrium. In Figure 5d, we summarize the saturated n-type core radius as a function of the nanowire radius and N_d.

The nonequilibrium situation here is similar to that of a p-n junction with a finite forward bias voltage.[1] With the criterion for saturation as a depletion time of 10^5 s, the band bending or diffusion barrier at saturation is ~1.3 eV. That is, the kinetic effects limit band bending to just about a third of the band gap

dx.doi.org/10.1021/am201633x | ACS Appl. Mater. Interfaces 2012, 4, 1365–1370

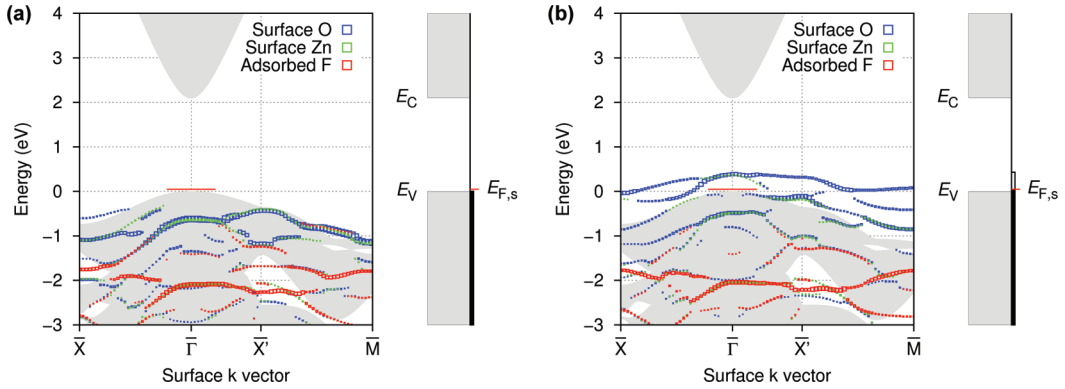

Figure 6. Spin-resolved band structure of the fully F-adsorbed ZnO $(10\bar{1}0)$ surface: Half-metallic surface electronic structures. (a) Majority-spin band structure. (b) Minority-spin band structure. The majority-spin bands of the oxygen-derived surface states are fully occupied. The minority-spin surface bands are metallic.

(3.4 eV) at room temperature. Thermal equilibrium that is tacitly assumed in discussion of electronic structures of semiconductor nanostructures,[45,46] therefore could be invalid for high bandgap semiconductors with high band bending, suggesting the need of reinterpreting the energy levels of surface defects in previous experiments on nanowire devices.[47−49]

Magnetic Structures. We now discuss the magnetic property of F-adsorbed ZnO surfaces. The spin-resolved surface band structure in Figure 6 shows that it is half-metallic: The majority-spin surface bands are fully occupied and stabilized below the surface Fermi level, and the minority-spin surface bands are partially occupied. The magnetic moment per surface unit cell is 0.993 μ_B, with 80 and 10% of which being derived from O and Zn atoms of the surface ZnO double layer, respectively, and the remaining 10% from deeper layers. It is consistent with half-filling of oxygen dangling orbital states, as depicted in Figure 3. The energy gain by spin polarization is 92 meV per surface unit cell. Calculations with double-size unit cells show that the ferromagnetic ordering is favored over the antiferromagnetic one along the ZnO dimer ($\langle 0001 \rangle$) direction by 27 meV and along the dimer row ($\langle 11\bar{2}0 \rangle$) direction by 54 meV. Adopting a nearest-neighbor Heisenberg exchange model $H=-\sum J_{ij}S_iS_j$ with $S = 1/2$, the Curie temperature can be estimated by $T_C = \eta S(S+1)\text{-}(z_{\|}J_{\|}+z_{\perp}J_{\perp})/3k_B$, where z's and J's are the coordination number and exchange constant for the directions parallel with and perpendicular to the dimer direction, and η is the T_C reduction factor for a two-dimensional square lattice, 0.57, to correct the error due to the mean field approximation.[50] With the values of $z_{\|} = z_{\perp} = 2$, $J_{\|} = 54$ meV and $J_{\perp} = 108$ meV, T_C for the present surface ferromagnetism is as high as 535 K.

The origin of the strong surface ferromagnetism can be understood with the Stoner model for the surface band. In the Stoner model,[51] ferromagnetism occurs when an exchange energy gain is higher than a kinetic energy cost, or, $J > N(E_F)^{-1}$. Here, J is the exchange interaction strength and $N(E_F)$ is the density of states at the Fermi level. This model has been used to explain the calculated ferromagnetism of B-, C-, or N-doped metal oxides,[52,53] B-doped diamond,[54] and hole-doped ZnO bulk,[55] in which the localized 2p orbitals of first-row atoms are responsible for the magnetism. For the F-adsorbed ZnO surface, the prominent surface band derived from O 2p orbitals has a narrow bandwidth of ~0.5 eV (Figure 6b) because of the reduced coordination at the surface. The density of states, which is approximately the inverse bandwidth, is therefore large enough to satisfy the Stoner criterion. We note that this surface ferromagnetism from partial emptying of oxygen-derived surface states may also be responsible for the intrinsic ferromagnetism of oxide nanostructures.[29−32]

Applications. The present postgrowth engineering of surface states is useful for photonic and photovoltaic applications of ZnO. One example is light emitting diodes (LED) that are made of a vertically aligned nanowire array with top and bottom electrodes. Such a nanowire LED was fabricated with GaN by growing the lower half of nanowires in n-type and the upper one in p-type via impurity doping, and showed a good performance.[56] Although ZnO is the best material for such an application, the p-type doping difficulty has hindered it. Our approach of postgrowth gas exposure enables to make ZnO nanowire LEDs. After growing the lower half of nanowires in n-type and the upper one in undoped or lightly n-type, an insulating high molecule such as a thin photoresist is spin-coated to fill a space of the lower half of the nanowire array, and then a fluorine gas is exposed. In this way, one can apply p-type surface transfer doping only to the upper half of nanowires. Another example is coaxial nanowire p-n junction devices for photovoltaic applications.[57,58] As discussed, thick n-type doped nanowires form coaxial p−n junctions naturally by p-type surface transfer doping. The thickness and n-type doping concentration are controllable variables for high performance.

Our postgrowth surface treatment is also useful for ZnO-based spintronic devices. While the surface ferromagnetism of the fluorine-adsorbed ZnO surface is useful by itself, it may give synergistic effects when it is combined with bulk doping of magnetic impurities. The demonstration of hole-mediated ferromagnetism for magnetic-impurity-doped ZnO is hindered by the p-type doping difficulty. Surface transfer p-type doping provides hole carriers near the surface and thereby could allow hole-mediated ferromagnetism. The formation of this p-type ferromagnetic semiconductor can be used to define ferromagnetic electrodes of all-semiconductor spin field-effect transistors (FET).[59]

CONCLUSION

Using first-principles and band diagram calculations, we showed that the postgrowth fluorine gas exposure for ZnO nanowires is an efficient way to make p-type doping of ZnO nanostructures. We also identified the kinetic control regime of the p-type transfer doping for unintentionally n-type doped nanowires,

warning that the thermal equilibrium condition is invalid in some cases. We finally showed that the fluorine adsorbed ZnO surface is ferromagnetic. The present surface treatment method can be used to make devices such as nanowire-array LEDs, coaxial photovoltaic devices and planar spin FETs.

AUTHOR INFORMATION

Corresponding Author

*E-mail: sung-hoon.lee@samsung.com.

Notes

The authors declare no competing financial interest.

ACKNOWLEDGMENTS

We thank Ju-Jin Kim, Young-Gu Jin, Hyo Sug Lee, and Sungil Park for helpful discussions.

REFERENCES

(1) Sze, S. M.; Ng, K. K. *Physics of Semiconductor Devices*, 3rd ed.; John Wiley & Sons: Hoboken, NJ, 2007.
(2) Huang, M. H.; Mao, S.; Feick, H.; Yan, H.; Wu, Y.; Kind, H.; Weber, E.; Russo, R.; Yang, P. *Science* **2001**, *292*, 1897−1899.
(3) Wang, Z. L. *Mater. Today* **2004**, *7*, 26−33.
(4) Lu, W.; Lieber, C. M. *Nat. Mater.* **2007**, *6*, 841−850.
(5) Yang, P.; Yan, R.; Fardy, M. *Nano Lett.* **2010**, *10*, 1529−1536.
(6) Hong, K.-H.; Kim, J.; Lee, S.-H.; Shin, J. K. *Nano Lett.* **2008**, *8*, 1335−1340.
(7) Hong, K.-H.; Kim, J.; Lee, J. H.; Shin, J.; Chung, U.-I. *Nano Lett.* **2010**, *10*, 1671−1676.
(8) Ristein, J. *Science* **2006**, *313*, 1057−1058.
(9) Zhang, P.; Tevaarwerk, E.; Park, B.-N.; Savage, D. E.; Celler, G. K.; Knezevic, I.; Evans, P. G.; Eriksson, M. A.; Lagally, M. G. *Nature* **2006**, *439*, 703−706.
(10) Calzolari, A.; Ruini, A.; Catellani, A. *J. Am. Chem. Soc.* **2011**, *133*, 5893−5899.
(11) Look, D. C. *Mater. Sci. Eng., B* **2001**, *80*, 383−387.
(12) Pearton, S. J.; Norton, D. P.; Ipa, K.; Heo, Y. W.; Steiner, T. *Prog. Mater. Sci.* **2005**, *50*, 293−340.
(13) Özgür, U.; Alivov, Y. I.; Liu, C.; Teke, A.; Reshchikov, M. A.; Doğan, S.; Avrutin, V.; Cho., S.-J.; Morkoç, H. *J. Appl. Phys.* **2005**, *98*, 041301.
(14) Park, C. H.; Zhang, S. B.; Wei, S.-H. *Phys. Rev. B* **2002**, *66*, 073202.
(15) Tsukazaki, A.; Ohtomo, A.; Onuma, T.; Ohtani, M.; Makino, T.; Sumiya, M.; Ohtani, K.; Chichibu, S. F.; Fuke, S.; Segawa, Y.; Ohno, H.; Koinuma, H.; Kawasaki, M. *Nat. Mater.* **2005**, *4*, 42−46.
(16) Xiang, B.; Wang, P.; Zhang, X.; Dayeh, S. A.; Aplin, D. P. R; Soci, C.; Yu, D.; Wang, D. *Nano Lett.* **2007**, *7*, 323−328.
(17) Yuan, G. D.; Zhang, W. J.; Jie, J. S.; Fan, X.; J. A. Zapien, L. B. L.; Leung, Y. H.; Wang, P. F.; Lee, C. S.; Lee, S. T. *Nano Lett.* **2008**, *8*, 2591−2597.
(18) Janotti, A.; Van de Walle, C. G. *Rep. Prog. Phys.* **2009**, *72*, 126501.
(19) McCluskey, M. D.; Jokela, S. J. *J. Appl. Phys.* **2009**, *106*, 071101.
(20) Dietl, T.; Ohno, H.; Matsukura, F.; Cibert, J.; Ferrand, D. *Science* **2000**, *287*, 1019−1022.
(21) Sato, K.; Bergqvist, L.; Kudrnovský, J.; Dederichs, P. H.; Eriksson, O.; Turek, I.; Sanyal, B.; Bouzerar, G.; Katayama-Yoshida, H.; Dinh, V. A.; Fukushima, T.; Kizaki, H.; Zeller, R. *Rev. Mod. Phys.* **2010**, *82*, 1633−1690.
(22) Toyoda, M.; Akai, H.; Sato, K.; Katayama-Yoshida, H. *Physica B* **2006**, *376*, 647−650.
(23) Sharma, P.; Gupta, A.; Rao, K. V.; Owens, F. J.; Sharma, R.; Ahuja, R.; Guillen, J. M. O.; Johansso, B.; Gehring, G. A. *Nat. Mater.* **2003**, *2*, 673−677.
(24) Radovanovic, P. V.; Gamelin, D. R. *Phys. Rev. Lett.* **2003**, *91*, 157202.
(25) Kittilstved, K. R.; Liu, W. K.; Gamelin, D. R. *Nat. Mater.* **2006**, *5*, 291−297.
(26) Zhang, Z. H.; Wang, X.; Xu, J. B.; Muller, S.; Ronning, C.; Li, Q. *Nature Nanotechnol* **2009**, *4*, 523−527.
(27) Pan, F.; Song, C.; Liu, X.; Yang, Y.; Zeng, F. *Mater. Sci. Eng., R* **2008**, *62*, 1−35.
(28) Dietl, T. *Nat. Mater.* **2010**, *9*, 965−974.
(29) Sundaresan, A.; Bhargavi, R.; Rangarajan, N.; Siddesh, U.; Rao, C. N. R. *Phys. Rev. B* **2006**, *74*, 161306.
(30) Gao, D.; Zhang, Z.; Fu, J.; Xu, Y.; Qi, J.; Xue, D. *J. Appl. Phys.* **2009**, *105*, 113928.
(31) Yan, Z.; Ma, Y.; Wang, D.; Wang, J.; Gao, Z.; Wang, L.; Yu, P.; Song, T. *Appl. Phys. Lett.* **2008**, *92*, 081911.
(32) Podila, R.; Queen, W.; Nath, A.; Arantes, J. T.; Schoenhalz, A. L.; Fazzio, A.; Dalpian, G. M.; He, J.; Hwu, S. J.; Skove, M. J.; Rao, A. M. *Nano Lett.* **2010**, *10*, 1383−1386.
(33) Erwin, S. C.; Himpsel, F. J. *Nat. Commun.* **2010**, *1*, 58.
(34) Joo, J.; Chow, B. Y.; Prakash, M.; Boyden, E. S.; Jacobson, J. M. *Nat. Mater.* **2011**, *10*, 596−601.
(35) Meyer, B.; Marx, D. *Phys. Rev. B* **2003**, *67*, 035403.
(36) Spicer, W. E.; Chye, P. W.; Skeath, P. R.; Su, C. Y.; Lindau, I. *J. Vac. Sci. Technol.* **1979**, *16*, 1422−1433.
(37) Van de Walle, C. G.; Segev, D. *J. Appl. Phys.* **2007**, *101*, 081704.
(38) Strobel, P.; Riedel, M.; Ristein, J.; Ley, L. *Nature* **2004**, *430*, 439−441.
(39) Perdew, J. P.; Burke, K.; Ernzerhof, M. *Phys. Rev. Lett.* **1996**, *77*, 3865−3868.
(40) Kresse, G.; Furthmüller, J. *Phys. Rev. B* **1996**, *54*, 11169−11186.
(41) Kresse, G.; Joubert, D. *Phys. Rev. B* **1999**, *59*, 1758−1775.
(42) Liechtenstein, A. I.; Anisimov, V. I.; Zaanen, J. *Phys. Rev. B* **1995**, *52*, R5467−R5470.
(43) Janotti, A.; Van de Walle, C. G. *Nat. Mater.* **2007**, *6*, 44−47.
(44) Singh, A. K.; Janotti, A.; Scheffler, M.; Van de Walle, C. G. *Phys. Rev. Lett.* **2008**, *101*, 055502.
(45) Björk, M. T.; Schmid, H.; Knoch, J.; Riel, H.; Riess, W. *Nature Nanotechnol.* **2009**, *4*, 103−107.
(46) Gao, X. P. A; Zheng, G.; Lieber, C. M. *Nano Lett.* **2010**, *10*, 547−552.
(47) Richter, T.; Meijers, H. L. R.; Calarco, R.; Marso, M. *Nano Lett.* **2008**, *8*, 3056−3059.
(48) Hong, W.-K.; Sohn, J. I.; Hwang, D.-K.; Kwon, S.-S.; Jo, G.; Song, S.; Kim, S.-M.; Ko, H.-J.; Park, S.-J.; Welland, M. E.; Lee, T. *Nano Lett.* **2008**, *8*, 950−956.
(49) Maeng, J.; Park, W.; Choe, M.; Jo, G.; Kahng, Y. H.; Lee, T. *Appl. Phys. Lett.* **2009**, *95*, 123101.
(50) Ashcroft, N. W.; Mermin, N. D. *Solid State Physics*; Brooks/Cole: Stamford, CT, 1976
(51) Stoner, E. C. *Proc. R. Soc. London, Ser. A* **1938**, *165*, 372−414.
(52) Kenmochi, K.; Dinh, V. A.; Sato, K.; Yanase, A.; Katayama-Yoshida, H. *J. Phys. Soc. Jpn.* **2004**, *73*, 2952−2954.
(53) Kenmochi, K.; Seike, M.; Sato, K.; Yanase, A.; Katayama-Yoshida, H. *Jpn. J. Appl. Phys.* **2004**, *43*, L934−L936.
(54) Kenmochi, K.; Sato, K.; Yanase, A.; Katayama-Yoshida, H. *Jpn. J. Appl. Phys.* **2005**, *44*, L51−L53.
(55) Peng, H.; Xiang, H. J.; Wei, S.-H.; Li, S.-S.; Xia, J.-B.; Li, J. *Phys. Rev. Lett.* **2009**, *102*, 017201.
(56) Kim, H.-M.; Cho, Y.-H.; Lee, H.; Kim, S. I.; Ryu, S. R.; Kim, D. Y.; Kang, T. W.; Chung, K. S. *Nano Lett.* **2004**, *4*, 1059−1062.
(57) Tian, B.; Zheng, X.; Kempa, T. J.; Fang, Y.; Yu, N.; Yu, G.; Huang, J.; Lieber, C. M. *Nature* **2007**, *449*, 885−889.
(58) Dong, Y.; Tian, B.; Kempa, T. J.; Lieber, C. M. *Nano Lett.* **2009**, *9*, 2183−2187.
(59) Žutić, I.; Fabian, J.; Das Sarma, S. *Rev. Mod. Phys.* **2004**, *76*, 323−410.